Available online at http://ijcpe.uobaghdad.edu.iq and www.iasj.net
Iraqi Journal of Chemical and Petroleum Engineering
Vol. 24 No.1 (March 2023) 13 – 26
EISSN: 2618-0707, PISSN: 1997-4884

Effect of Heterogeneity on Capillary Pressure and Relative Permeability Curves in Carbonate Reservoirs. A Case Study for Mishrif Formation in West Qurna/1 Oilfield, Iraq

Ahmed N. Al-Dujaili [a], Mehdi Shabani [a, *], and Mohammed S. AL-Jawad [b]

a AmirKabir University of Technology, Petroleum Engineering Department, Iran
b Petroleum Engineering Department, College of Engineering, University of Baghdad, Iraq

Abstract

The special core analysis tests were accomplished on a set of core plugs for Mishrif Formation (mA, mB1, and mB2cde/mC units) in West Qurna/1 oilfield, southern Iraq. Oil relative permeability (K_{ro}) data and the Corey-type fit of the data as functions of the brine saturation at the core outlet face for individual samples in the water-oil imbibition process to estimate relative permeability measurements by the centrifuge method were utilized. Identical correlations for oil and water relative permeabilities were extracted by steady-state and unsteady-state methods. For the mA samples, the gas-water capillary pressure curves were within a narrow range (almost identical) indicating that mA is a homogeneous unit. Kro curves for three mB2ab plugs were practically identical, that is referring to the homogeneity in the upper portion of the unit. The mB2 unit has a more solid-phase concentration than other units. In addition, the general trend of low residual oil saturation is related to the raising in porosity but no reliable correlation between the residual oil saturation to water drive (S_{orw}) and Klinkenberg-corrected permeability (K_{inf}). Based on the correlation between the effective oil permeability at the initial water saturation [ko(Swi)] and (K_{inf}/f)1/2 for the high-permeability lithofacies mB1 plugs, $k_o(S_{wi})$ is approximately equal to or exceeds K_{inf}. While k_o(Swi) was below K_{inf} for the other samples. New good empirical equations were obtained for effective gas permeability at final water saturation versus K_{inf}, as well as, for K_{ro} and K_{rw} versus saturation for all lithofacies.

Keywords: Heterogeneity; Relative Permeability; Capillary Pressure; Mishrif; West Qurna; secondary recovery, wettability.

Received on 03/08/2022, Received in Revised Form on 29/08/2022, Accepted on 31/08/2022, Published on 30/03/2023

https://doi.org/10.31699/IJCPE.2023.1.3

1- Introduction

Apparent sedimentary rock features were the main source of data and predictive interpretations applications for underground exploration and expansion of the hydrocarbon industry [1]. Since the middle of the 12th century, cores studies were growly to comprehend: a-the reservoir structure, b- formation units according to available seismic information, and c- to assess cores studies' effectiveness on production techniques [2]. The realization of the heterogeneity impact on reservoirs production, and with supported by computer analysis and map techniques, core studies have transitioned into a more quantitative value with a view to output a formation physical properties in the form of statistical data and deterministic models to understand the reservoir conditions in the right way [3].

Furthermore, appropriate reservoir simulation needs immobile properties, such as porosity and permeability, and also requires knowing the more effective properties like (saturation (S), capillary pressure (Pc), and relative permeability (Kr)) anywhere in the certain reservoir [4, 5]. Although the well sites can give most of the required properties calculations, also there is a need to estimate these values related to interested zones. Since the instant imbibition has a controlling role in the hydrocarbon reservoirs recovery (especially under aqueous flooding and naturally fractured reservoirs), the results of the spontaneous imbibition experiment must be scaled-up to improve the reservoir mechanisms' performance [6]. However, some studies had been not focused on expanding the dynamic properties of a reservoir. It is assumed that these properties are a function of rock types that are categorized by φ, K, Kr, and Pc [7]. When the distribution of different rocks and the exact boundaries in the reservoir are known, then the dynamic properties for each block in the simulation process can be calculated easily [8].

1.1. Capillary pressure and heterogeneity

The capillary pressure represents the calculation of the two-phase pressures differences in the fluid interface [9]. Many studies exhibited that the surface tension between the fluids, rock wettability, distribution of pore size, as well as temperature represent the main factors on which capillary pressure depends (Bear 2018). The young-

*Corresponding Author: Name: Mehdi Shabani, Email: mehdi.shabani@aut.ac.ir

Laplace equation represents the capillary pressure easily as below [10]:

$$P_c = \frac{2\sigma cos\theta}{r_c} \quad (1)$$

Where: P_c is the capillary pressure (psi), θ is the contact angle, σ is the interfacial tension (lb/in), and *rc* is the effective radius of porous media (in).

When (S = 1), the capillary pressure may be equal to zero (Fig. 1 – left) or at a positive value (Fig. 1 – right). This pressure represents the bubbling pressure or threshold pressure, or non-wetting phase value [11]. Initially, when the medium is saturated by wetting fluid, it reflects the minimum pressure for a non-wetting fluid entering into the medium. Capillary pressure curves typically are obtained if the threshold pressure is equal to zero [12]. If the saturation on one side of the interface has existed, also that will lead to the existence of corresponding saturation on the other side in a way that the capillary pressure will be continuous. In this case, the second interface condition represents just the continuity of capillary pressure. Continuity of capillary pressure can be accomplished when the threshold saturation (S*) is possible to exist, the threshold pressure is positive, and the wetting phase saturation on the corresponding side for the lower curve is below or equal to S* but not above this value [13].

1.2. Relative permeability

Relative permeability (Kr) is an indicator of rocks and the chemical and physical properties of the fluids. (Kr) is affected by temperature change and the rocks and liquids relative wetting phase [14]. The temperature will be more effective on relative permeability when water, oil, and rock in the system become more humid when the temperature rises [15, 16]. Three liquids (gas, oil, and water) may exist and move in the rock system and at a definite saturation, so three-phase relative permeabilities must be taken into consideration [17]. The traditional method for estimation the 3-phases Kr has not to be certain. Several papers discussed this but conflicted in attention either to data or to the procedures [18]. On the other hand, methods for determining the Kr for 2-phases (gas - oil, gas - water, water-oil) are well laid out. Two methods were considered, the steady state, which in this method and at constant flow rates, two liquids are to flow in and out of the core at many saturation values, and the unsteady-state which two liquids that saturate a core with either gas or water can be displaced. The definition of (Kr) is as follows [19]:

$$k_{rg=}\, k_{eg}/k\,;\, k_{rw=}\, k_{ew}/k\,;\, k_{ro=}\, k_{eo}/k \quad (2)$$

Where: k_{rg}, k_{ro},and k_{rw} represent gas, oil, and water relative permeabilities respectively; k_{eg}, k_{eo}, and k_{ew}: Gas, oil, and water effective permeabilities respectively(md); k is the absolute permeability(md).

Saturation, saturation history, Pore geometry, viscosity, wettability, temperature, capillary, and gravitational intensities are the parameters affected on Kr [20]. In an oil-water system, Kro and Krw are usually drawn as a function of Sw as idealistically, shown in Fig. 1.

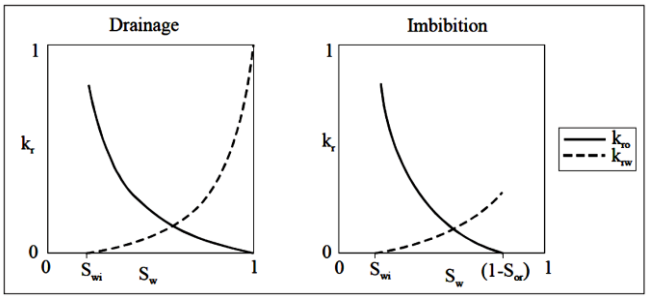

Fig. 1. Kro and Krw Versus Sw [8]

The drainage and imbibition represent curves that point directions out the saturation histories. The drainage curve identifies the wetting phase as decreasing (saturation decreasing), while the imbibition curve will identify the case of saturation increase [8]. Kr curves are controlled by three elements:

1. Endpoint saturations.
2. Endpoint permeabilities.
3. Bending of Kr.

Leverett J saturation unique function (Eq. 3) has been created. In a water-wet state and for many different incompact grains of sand, it is found that a single characteristic curve has been existed [21, 22].

$$J_{(SW)} = \frac{P_c}{2\sigma\cos\theta}\sqrt{\frac{k}{\varphi}} \quad (3)$$

Where: k is the absolute permeability, P_c is the capillary pressure (psi), σ is the interfacial tension (psi), θ is the contact angle,$(K/\varphi)^{1/2}$ is interpreted as a grain diameter or characteristic mean pore.

Eq. 3 is simple and gives Kr data for the entire saturation range that give advantages of this method [23].

- Relative Permeability Models

1. Normalized Saturation (NSF)

When the capillary number or the saturation history changes, the residual saturation will change [24]. In the same way, Kr and Pc curves will change also (Baker 1988). It is ordinary that the NSF equation is utilized (Eq. 4) to represent Kr and Pc curves [25, 26].

$$S = \frac{(S_w - S_{wi})}{(1 - S_{or} - S_{wi})} \quad (4)$$

Where: Sw is water saturation (Frac.); S_{wi} is the initial water saturation (Frac.); S_{or} is residual oil saturation (Frac.).

2. Non-wetting Model

According to Corey's assumptions, the Kr of the wetting phase can be modified utilizing the power law. Thus, the

Kr reduction in the non-wetting phase must be expected at high saturation values to correspond with the miniature wetting phase saturation. At the values, more and less than the non-wetting saturation (Sx) [27], all types of behavior must incorporate in one Kr curve without cutout [28]. The model compatible with all these requirements will be represented in the set of the following equations:

$$K_{rnw}(S_{nw}) = K^{0}_{rnw}[1.0 - (1.0 - S)^{m(s)}]^{n(s)} \quad (5)$$

$$S = \frac{(S_{nw} - S_{nwr})}{(S_{nwi} - S_{nwr})} \quad (6)$$

$$SS = \frac{(S_x - S_{nwr})}{S_{nwi} - S_{nwr})} \quad (7)$$

$$IF\ (S < SS)\ THEN$$

$$n(S) = n_0 \quad (8)$$

$$m(S) = 1 \quad (9)$$

$$ELSE$$

$$n(S) = n_0 - (n_0 - 1.0)\{\frac{(S-SS)}{1.0-SS)}\}^2 \quad (10)$$

$$m(S) = 1 + (m_0 - 1.0)\{\frac{(S-SS)}{1.0-SS)}\}^2 \quad (11)$$

Where: Sx is non-wetting saturation (frac.), n is the displacing fluid, m_o is exponent for wetting phase (dimensionless), n_o is Corey exponent for non-wetting phase (dimensionless).

3. Unsteady and steady state methods

Unsteady State Method**:** This method is based on: a- the Buckley-Leverett for two-phase displacement, b-the Welge method to estimate outflow end saturation from the cumulative production, c- the Johnson-Bossler- Neumann method to estimate each individual Kr value rather than the ratio using the pressure information.

Steady-State Method: The steady state is the most precise method for calculating relative permeability. The only disadvantage represented in supplies and mechanism used. Equipment is so complicated and the measurements are time exhaustion [29].

1.3. Geological setting

Iraqi supergiant oil fields are located mainly in southern Iraq. One of these is West Qurna in Northwestern Basra city, and it is evaluated to contain approximately 30 to 40 billion barrels of regaining reserves [30].

The West Qurna/1oil field has existed in the Southern Mesopotamian Basin neighboring the Eastern edge of the Arabian plate (Fig. 2) located within the Zubair Subzone and structurally, a part of a large isocline towards the North [31]. Geographically, it is located 50 km Northwest of Basra City and extends 29 km long and 17 km wide. The West Qurna oilfield represents the Northern expansion of the supergiant Rumaila field [32].

Fig. 2. Location of West Qurna/1 oil field [31]

1.4. Mishrif Reservoir

The Mishrif Formation is known as a thick sequence of carbonate rocks that dominates almost 30% of oil reserves in Iraqi oilfields, consists of five units, CRI at the top of the formation, then mA, CRII, mB1, and mB2 at the bottom [29]. Mishrif Formation holds an irregular quality and heterogeneous reservoir properties by the effect of the depositional cycles and the sequence stratigraphic. Rocks porosity ranges from high porous (more than 20%) to low (5-10%) [33], the heterogeneity effect is very clear in variable permeability anisotropy values, in which the mb1 unit indicates more than the heterogeneity of the others [34].

2- Experimental Work

2.1. Materials and Methods

Special core analysis tests (gas-brine) primary drainage capillary pressure, Water-oil primary imbibition capillary pressure and relative permeability by the centrifuge method, Water-oil primary imbibition relative permeability by the steady-state method, and electrical properties were accomplished on a set of core plugs for the Mishrif reservoir (mA, mB1, and mB2cde/mC units) West Qurna/1 oilfield, Southern Iraq. Further, routine core analysis tests, tests were performed. The following tasks were performed (Table 1):

Table 1. Tests and Number of Samples and Tests for This Study

Item	Test	Number of Samples
1	Plug CT scan and oil permeability screening	234
2	Gas-water primary drainage capillary pressure and electrical property measurement by the porous plate method	12
3	Water-oil primary imbibition capillary pressure by the centrifuge method	16
4	Water-oil primary imbibition relative permeability by the centrifuge method	16
5	Water-oil primary imbibition relative permeability by the steady-state method	4

- Electrical properties

Electrical properties (cementation exponent and saturation exponent) for each sample were measured using Hassler and Brunner method, 1945. The plugs were from three units (mA, mB1, and mB2). The formation brine resistivity (Rw) at 0.044 ohm-m. Core sample resistivity (Ro) was measured at 100% of brine saturation. Formation factor (F) was computed using Ro and Rw method (Eq. 12).

$$F = \frac{R_o}{R_w} \quad (12)$$

The cementation (porosity) exponent (m) of each core plug was calculated using the equation:

$$m = \frac{logF}{log\varphi} \quad (13)$$

Where: Ro is core sample resistivity; Rw is formation brine resistivity.

2.2. Results

2.2.1. Capillary Pressure Data

The results of the gas-water primary drainage capillary pressure measurements for mA, mB1, and mB2 units are shown in Table 2 and Fig. 3.

Table 2. Gas-Water Primary Drainage Capillary Pressure for Lithofacies mA, mB_1, and mB_2

Unit	Porosity frac BV	Klinkenberg- gas permeability (mD.)	S_{wf} frac PV.	K_{eg} at final water saturation
mA	0.2030 – 0.2370	2.360 – 4.29	0.127 - 0.160	1.910 - 3.41
mB_1	0.1010 – 0.2510	1.230 – 99.2	0.089 - 0.301	0.782 - 62.3
mB_2	0.1800 – 0.2750	0.363 – 4.38	0.156 - 0.315	0.003 - 3.09

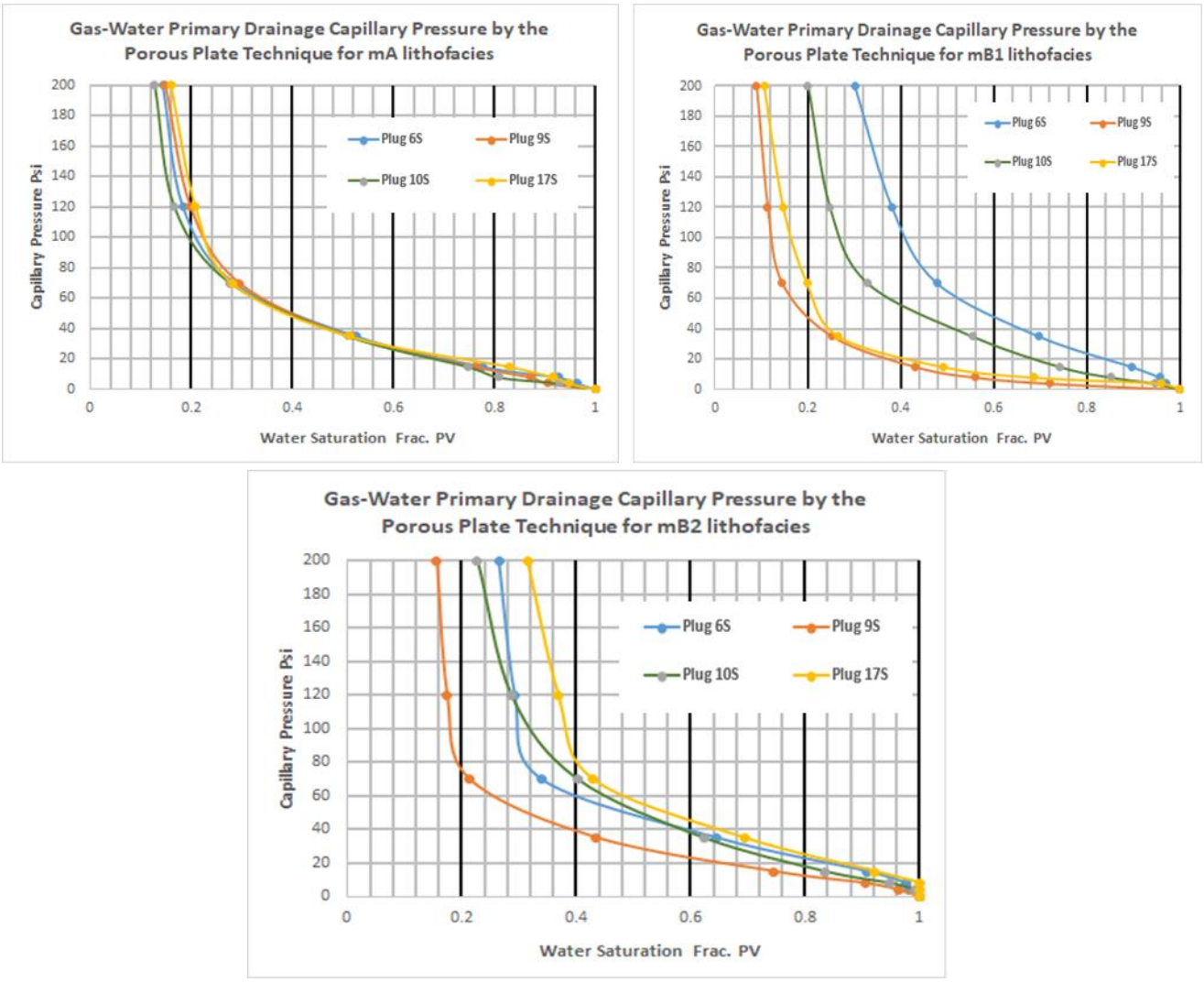

Fig. 3. Pc (Gas –Water) for mA, mB_1, and mB_2 Lithofacies

The test results for the mA plugs showed that the samples had porosity in the range (0.2030 – 0.2370) and the corrected Klinkenberg gas permeability (Kinf) in the range (2.36 – 4.29) mD. At the end of the capillary

pressure tests (at maximum gas-water capillary pressure of 200 psi), the final water saturation range will be from 0.127 to 0.160. Effective gas permeability at the final water saturation range is 1.91 to 3.41 mD. While the mB1 plugs porosity range is 0.1010 – 0.2510 and the Kinf range is between 1.23 – 99.2 mD. The final water saturation range is 0.0890 to 0.3010. Effective gas permeability at final water saturation is ranged from 0.782 to 62.3 mD.

The mB2cde/mC Plugs porosity is in the range 0.1800 – 0.2750 and Kinf in the range 0.363 – 4.38 mD. While the final water saturation range from 0.1560 to 0.3150. Effective gas permeability range at the final water saturation 0.003 to 3.09 mD.

2.2.2. Correlation between Effective Permeability at Final Water Saturation and K_{inf}

Fig. 4 shows effective gas permeability at final water saturation versus K_{inf}. The figure indicates a good correlation between $K_{g\ (Swi)}$ and K_{inf}.

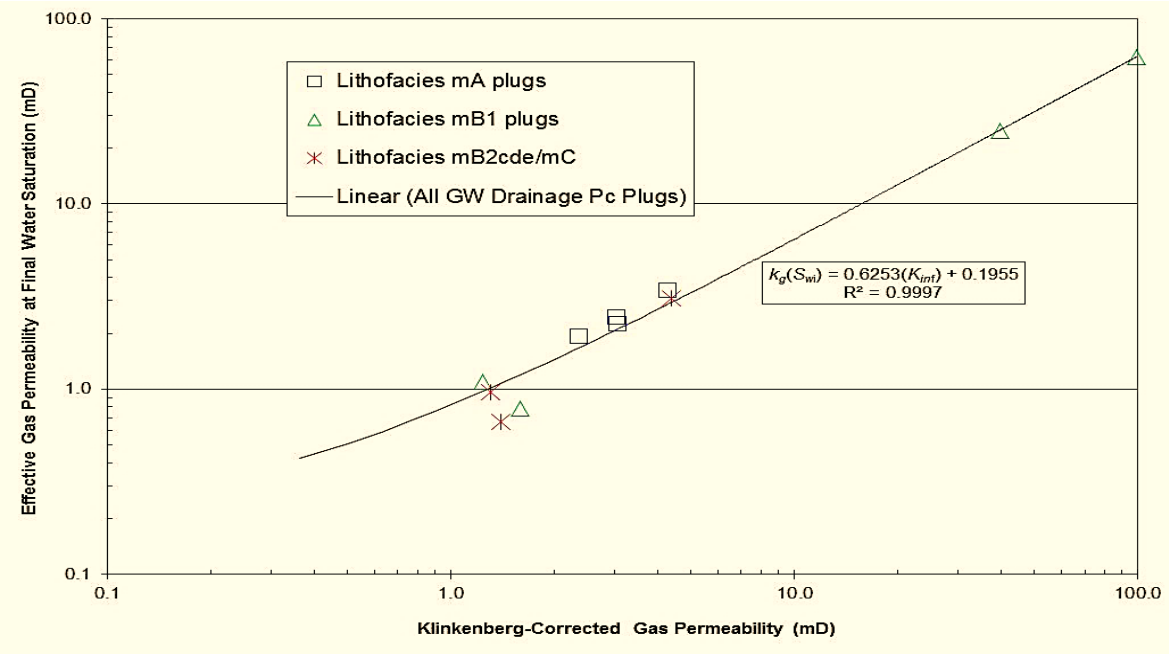

(A)

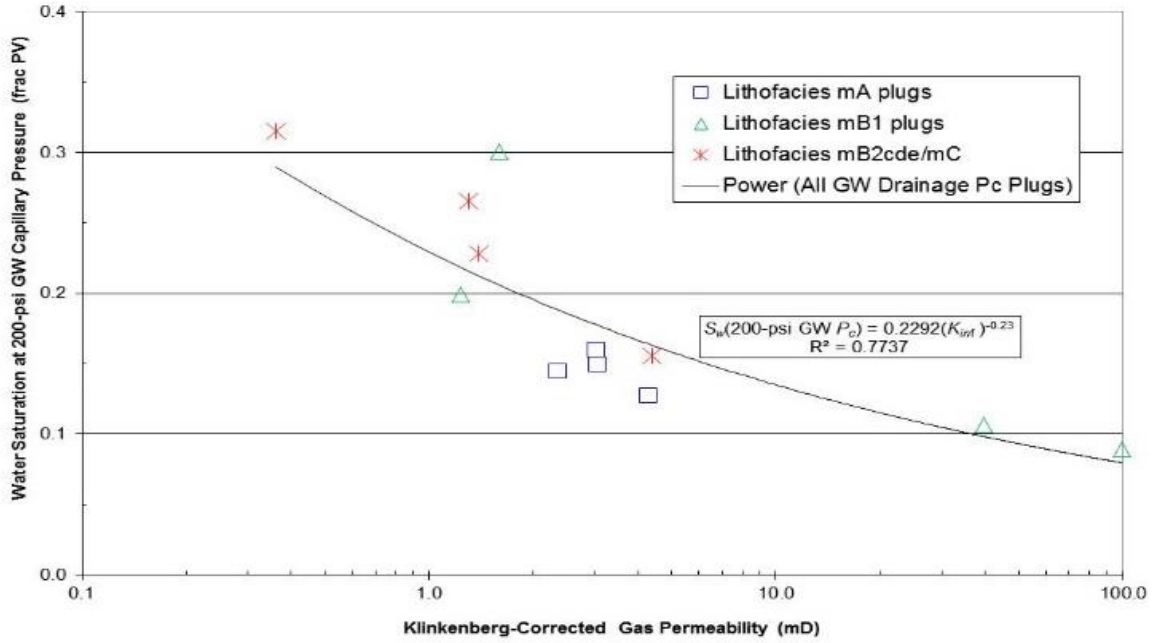

(B)

Fig. 4. A- K_{inf} Versus K_e at Fluid Water Saturation B- K_{inf} Versus Sw at Max. Water Gas Pc

2.2.3. Electrical properties

The summary of Electrical Properties Data by the Porous Plate Technique for Mishrif Reservoir in West Qurna/1 oilfield listed in Table 3.

Lithofacies mA Plugs: As shown in Table 1, the mA porosity is in the range 0.2030 – 0.2370. The formation resistivity factor (Fa) ranges between 18.72 and 28.36. The mA samples cementation exponent (m) range between 2.03 and 2.11. The saturation exponent (n) ranges between 1.70 and 1.85. Kinf of the samples in the range 2.36-4.29.

Lithofacies mB1 Plugs: The mB1 porosity extends over a wide range of 0.1010 – 0.2510. (Fa) ranges 14.51 to 120.48 for and the lowest at the highest porosity respectively. (m) ranges between 1.93 and 2.09 and (n) ranges between 1.77 and 2.06. Kinf of the mB1 plugs ranges between 1.23 and 99.2 mD.

Lithofacies mB2cde/mC Plugs: The porosity of the mB2ced/mC plugs in the range 0.1800 – 0.2750. (Fa) ranges between 13.88 and 35.50, (m) range between 2.03 and 2.20, and (n) range between 1.81 and 2.02. The Kinf of the plugs is between 0.363 and 4.38 mD.

Table 3. Electrical Properties Data by the Porous Plate Technique

Saturant (ppm)	216,988
Net Confining Stress (psi):	4000
Saturant resistivity, ohm-m at 25°C:	0.044
Porosity Exponent (m) [Composite]:	2.06
Y-Intercept(a):	1.00
Saturation Exponent (n) [Composite]:	1.89

Depth (m)	Layer	Grain Density (1) (g/cc)	Klink. Perm(1) (mD)	Porosity(1) (fraction BV)	Sw at Max Pc	Parameters determined from resist.		
						Fa	m	n
2259.35	mA	2.70	2.36	0.235	0.144	20.08	2.07	1.75
2259.80	mA	2.69	3.06	0.237	0.149	18.72	2.03	1.85
2259.89	mA	2.69	4.29	0.225	0.127	23.13	2.11	1.77
2273.11	mA	2.69	3.04	0.203	0.160	28.36	2.10	1.70
2289.02	mB1	2.68	1.59	0.170	0.301	35.44	2.01	1.77
2308.07	mB1	2.69	99.2	0.239	0.089	16.58	1.96	2.06
2318.53	mB1	2.70	1.23	0.101	0.199	120.48	2.09	2.06
2323.11	mB1	2.69	39.7	0.251	0.106	14.51	1.93	2.01
2354.67	mB2	2.69	1.30	0.223	0.265	21.08	2.03	1.81
2360.68	mB2	2.69	4.38	0.275	0.156	13.88	2.04	1.91
2365.19	mB2	2.69	1.39	0.198	0.228	35.50	2.20	2.02
2392.37	mB2	2.70	0.363	0.180	0.315	34.98	2.07	1.88

(1) Routine properties were measured after primary drainage capillary pressure tests

2.2.4. Water-Oil Imbibition Oil Capillary Pressure

The water-oil imbibition capillary pressure results summarized in Fig. 5. Fig. 6-A, B, and C show the oil saturation data at maximum centrifuge speed (near residual oil saturation) when plotted versus the petrophysical properties, such as absolute gas permeability, the porosity, and the pore throat characteristic $(K_{inf}/\phi)^{1/2}$. Fig. 6-A and B shows the general trend of lower near-residual oil saturation with higher porosity, but no reliable correlation neither between oil saturation at maximum water oil imbibition and Kinf nor with porosity. Fig. 6-C shows the effective oil permeability at initial water saturation [Ko(Swi)] versus Kinf. For higher-permeability lithofacies mB1 plugs, Ko(Swi) is nearly equal to or exceeds K_{inf}. Ko(Swi) is below Kinf for the remaining samples (lithofacies mA, mB2/ab, and mB2cde/mC). Fig. 6-D shows the relation between k_{eo} at initial water saturation and effective brine permeability at final water saturation.

2.2.5. Water-Oil Imbibition Kr by the Centrifuge Method

The water-oil imbibition relative permeability results shown in Table 4 and Fig. 7.

As shown in Fig. 7-C and D, K_{ro} curves for three mB_2ab plugs are practically identical.

Note that centrifuge relative permeability data at low water saturation (<0.4 frac PV) were not presented. One of the assumptions, associated with the centrifuge k_{ro} calculations, involves negligible flowing pressure gradient in the displacing (water) phase. This assumption is reasonable at high water saturation and it is violated at low water saturation. Therefore, k_{ro} data at Sw < 0.4 fraction were not included in the figure.

2.2.6. Water-Oil Primary Imbibition Kr by the Steady-State/Unsteady-State Method

Steady-state/unsteady-state (SS/USS) water-oil imbibition relative permeability data are used to obtain accurate data over a wide range of saturation for use in reservoir engineering calculations. The SS/USS measurements were performed on two composite core samples. The results as shown in Fig. 8. K_o values for mA, mB1, mB_2/ab, and mB_2/mc are 2.14, 58.48, 10.96, and 146.2 mD respectively.

The following correlations of K_{rw} and K_{ro} were extracted as in Table 5.

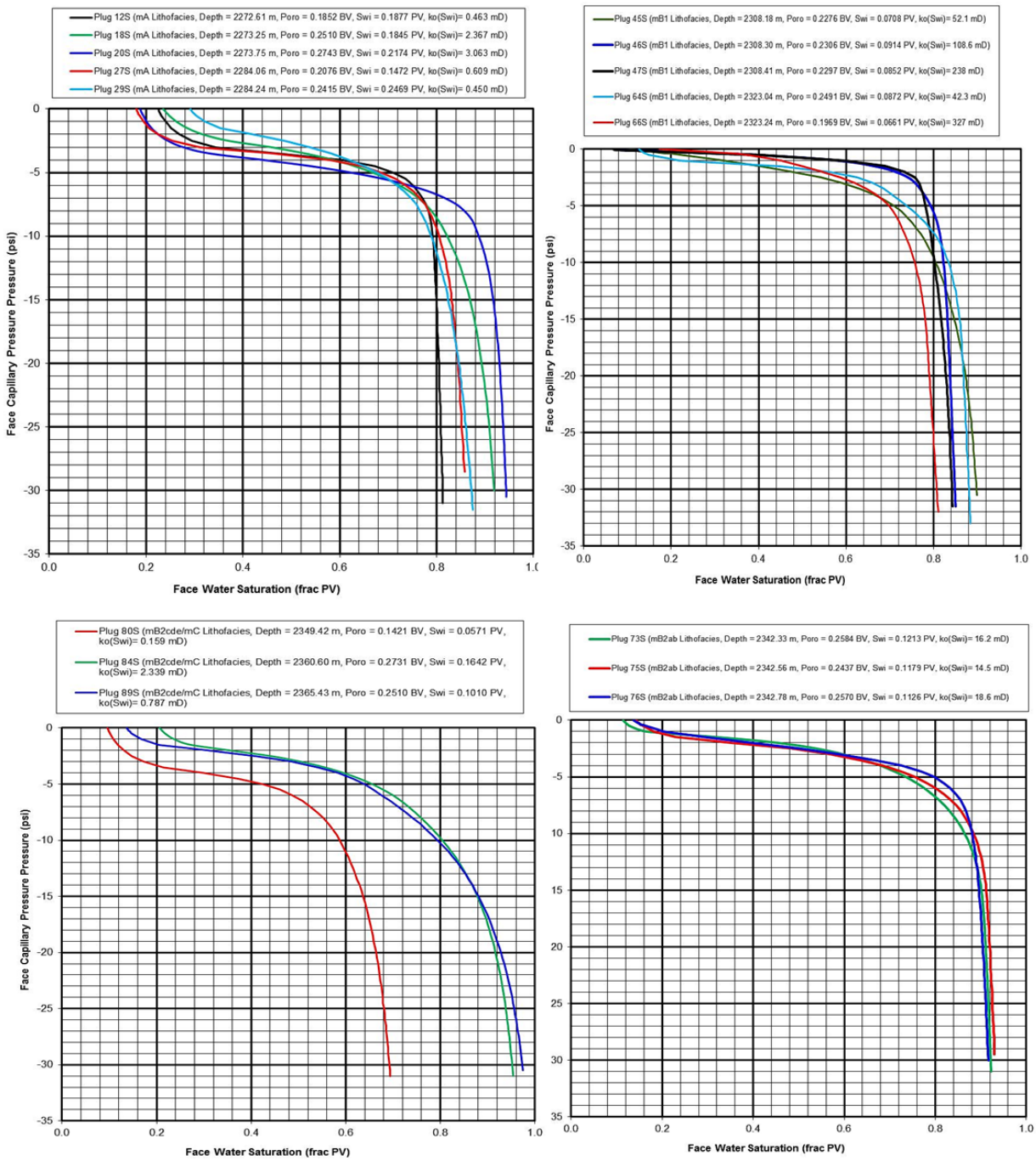

Fig. 5. (Water-Oil) Imbibition for mA, mB1, mB2ab, and mB2cde/mc

Table 4. Centrifuge Water-Oil Imbibition kr Measurements for Lithofacies mA, mB1, and mB2

Unit	S_{wi} frac. PV	Final outlet face So frac. PV	So at the end of the tests frac. PV	K_{rb} frac $ko_{(Swi)}$.	K_{eo} at S_{wi} mD.
mA	0.150 - 0.227	0.392 - 0.440	0.334 - 0.369	0.264 - 0.670	0.186 -1.787
mB_1	0.050 - 0.091	0.610 - 0.750	0.259 - 0.365	0.862 - 1.170	35.5 - 308.9
mB_2/ab	0.107 - 0.116	0.301 - 0.317	0.273 - 0.290	0.928 - 1.123	12.6 - 16.14
mB_2/mc	0.097 - 0.160	0.259 - 0.400	0.276 - 0.487	0.363 - 0.558	0.155 - 1.782

Table 5. Correlations of K_{rw} and K_{ro} versus water saturation by SS/USS Method

Unit	K_{rw} Versus Water saturation	R^2	K_{ro} Versus Water saturation	R^2
mA	$K_{rw} = 0.0002 * EXP[11.956 * (S_w)]$	0.9589	$K_{ro} = 3.7527 * EXP[-9.024 * (S_w)]$	0.9557
mB_1	$K_{rw} = 0.0010 * EXP[12.253 * (S_w)]$	0.8979	$K_{ro} = 2.4648 * EXP[-9.843 * (S_w)]$	0.9638
mB_2/ab	$K_{rw} = 0.0005 * EXP[14.018 * (S_w)]$	0.8788	$K_{ro} = 3.8926 * EXP[-9.360 * (S_w)]$	0.9721
mB_2/mc	$K_{rw} = 0.0003 * EXP[15.809 * (S_w)]$	0.8757	$K_{ro} = 4.2072 * EXP[-12.80 * (S_w)]$	0.9891

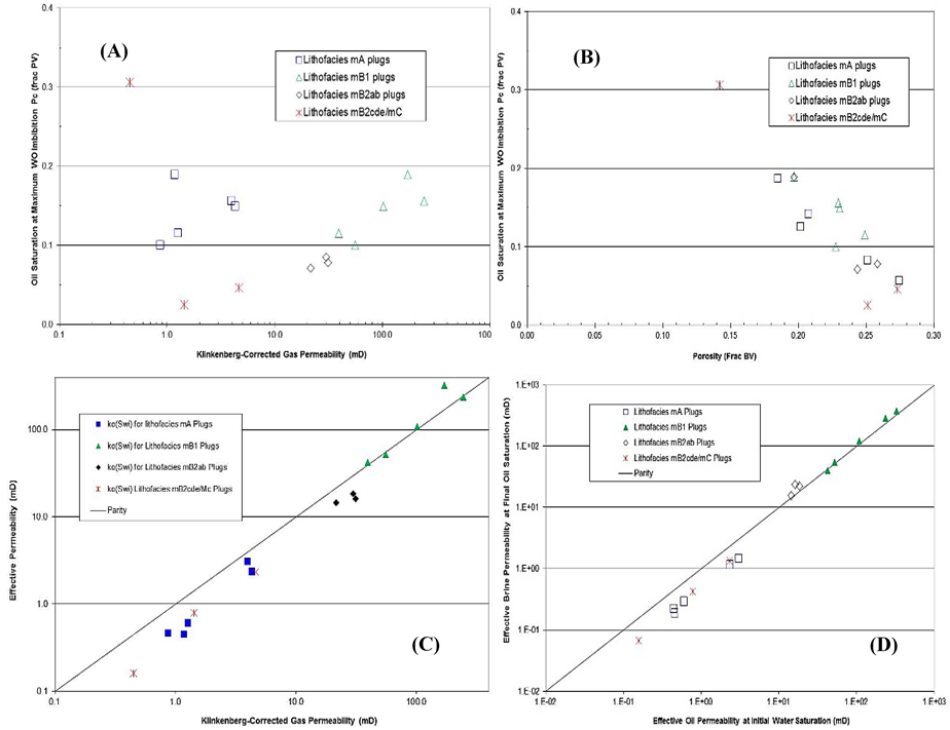

Fig. 6. A- K_{inf} Vs So at Max. Pc, B- φ Vs So at Max. Pc, C- K_{inf} Vs K_e, D- Keo Vs Ke of brine (All Lithofacies)

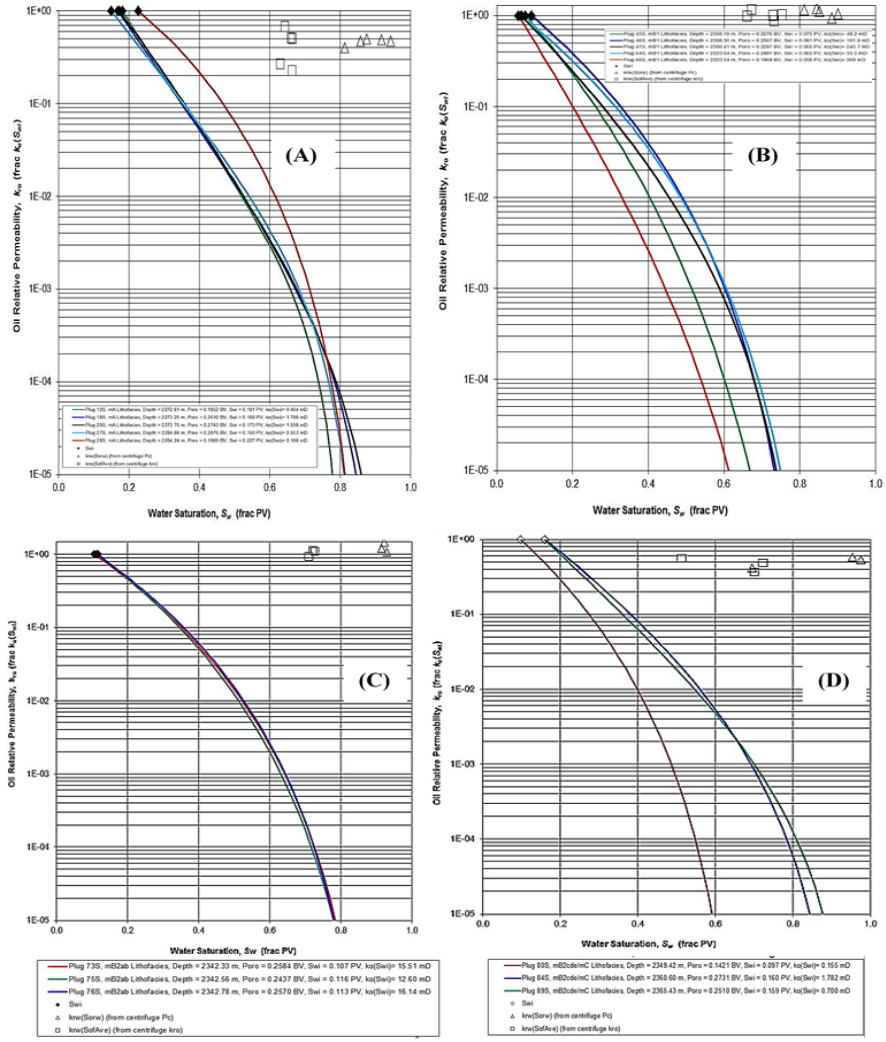

Fig. 7. K_{ro} (Water-Oil) Imbibition (A) for mA, (B) for mB1, K_{ro} (Water-Oil) Imbibition, (C) for mB_2/ab, and (D)

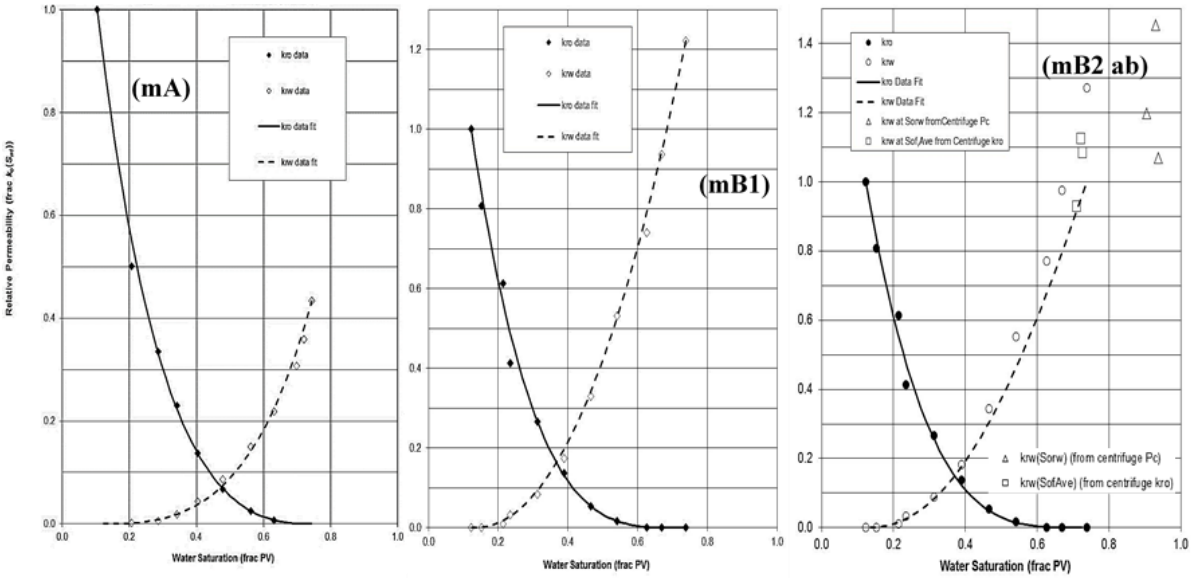

Fig. 8. Kr by the Steady-State/Unsteady-State Method for mA, mB1, and mB2ab Lithofacies from Left to Right Respectively

3- Discussion

For the mA samples, the gas-water capillary pressure curves fell within a narrow range (almost identical) as in Fig. 3, that's attributed to the narrow range of porosity and permeability in this unit, referring to some homogeneity. The results showed that (m) >2, which referred that the rocks of Mishrif consist of large dense grain. The mB2 unit consists of solid-phase concentration more than the others do.

According to Fig. 4-A, a good relationship between Kinf and Kg at final water saturation was noticed with a regression equal to 0.9997 and can be represented in the following form:

$$K_{g_{(S_{wi})}} = 0.6253(K_{inf}) + 0.1955 \quad (14)$$

Fig. 4-b showed a good relationship between Kinf and Sw at maximum capillary pressure value with a regression equal to 0.7737 and can be represented in the following form:

$$S_{w_{(max.P_c)}} = 0.2292(K_{inf})^{-0.23} \quad (15)$$

As can be seen in Fig. 5 for the mA samples, all curves tended to reach final face oil saturation values in the range of 0.046 to 0.187 of PV, while the (final face oil saturation) values for mB1 lithofacies were in the range of 0.100 to 0.189 of PV. Average oil saturation at the end of the centrifuge tests ranged between 0.198 and 0.262 of PV and the corresponding brine relative permeability ranged between 0.95 and 1.20. The (final face oil saturation) values for mB2/ab lithofacies were in the range of 0.071 to 0.085 of PV. Average oil saturation at the end of the centrifuge tests ranged between 0.193 and 0.195 of PV and the corresponding brine relative permeability ranged between 1.069 and 1.453, while the (final face oil saturation) values for mB2cde/mC lithofacies were in the range of 0.025 to 0.306 of PV. Average oil saturation at the end of the centrifuge tests ranged between 0.219 and 0.448 of PV and the corresponding brine relative permeability ranged between 0.418 and 0.577.

Fig. 6 (a, b, and c) illustrated that oil saturation at maximum centrifuge speed (near-residual oil saturation) plotted versus petrophysical properties such as absolute gas permeability, porosity, and the pore throat characteristic $(Kinf/\phi)^{1/2}$ for the samples tested. Fig. 6-C shows a general trend of lower near-residual oil saturation with higher porosity but no reliable correlation between near Sorw and Kinf nor $(Kinf,/\phi)^{1/2}$. For Water-Oil Imbibition Oil Capillary Pressure, the high water relative permeability at the near S_{orw} is indicative of oil wetting tendencies in the mB1 and mB2cde/mC samples. On the other hand, the k_w (S_{orw}^{Pc}) of the lower permeability lithofacies (mA and mB2ab) plugs is roughly 40-60% k_o (S_{wi}^{Pc}). This is indicative of mixed-wet tendencies in the mA and mB2ab samples.

The capillary pressure data depend on interfacial tension between the various fluid phases, so the interfacial tension data obtained under laboratory conditions must be adjusted to reservoir conditions. For Water-Oil Primary Imbibition Kr by the Centrifuge Method, as shown in Fig. 7-C, Kro curves for three mB2ab plugs were practically identical, that is referring to the homogeneity in the upper portion of the unit. The water saturation at the outlet face for the individual core plugs was less than the average water saturation in the primary sample with some exceptions. We do not have an explanation for this behavior.

Fig. 7-D shows that the kro curves for most plugs are practically identical but substantially differ from the kro curve for only one plug; this trend is similar to the centrifuge Pc trend, as shown in Fig. 5-D. We attribute

this to the lower porosity (0.1421) compared to the porosity of plugs (0.2731 and 0.2510, respectively).

Centrifuge relative permeability data at lower water saturation (<0.4) were not presented in Fig. 7. One of the assumptions associated with the centrifuge Kro calculations involves a negligible flowing pressure gradient in the displacing water phase. This assumption is reasonable at high water saturation and violated at low water saturation. Therefore, Kro data at Sw < 0.4 has not represented.

Fig. 9 provides a comparison between steady-state relative permeability and the centrifuge kro and endpoint data. In addition, Fig. 9 shows that the mA plugs near-residual oil saturations, obtained using water-oil imbibition capillary pressure tests.

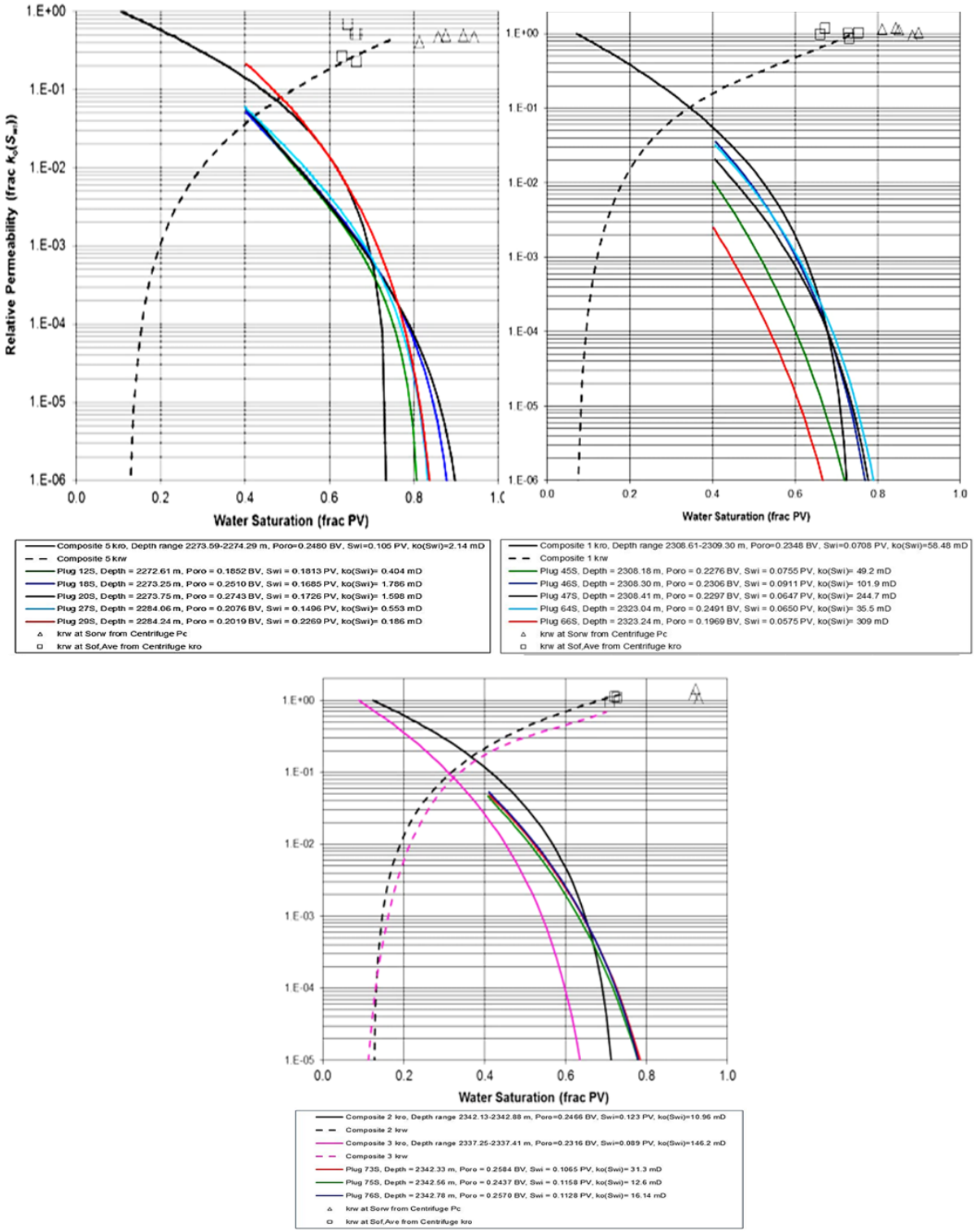

Fig. 9. Comparison Between Steady-State Relative Permeability and Centrifuge kro and Endpoint for mA, mB1, and mB2 Lithofacies

4- Conclusions

Six different models done to determine electrical properties, capillary pressure curves, and relative permeability for all Mishrif reservoir producible units in the West Qurna oil field by imbibition process. A variety of heterogeneous rocks was used using a wide range of plugs.

1- The conjunction between measurements of steady-state/unsteady state and centrifuge techniques will afford a preferable full Kr curve.
2- Gas-water capillary pressure curves of the four mA plugs fell within a narrow range. This phenomenon is attributed to the narrow range of porosity and permeability of the samples.
3- New good empirical equations are obtained for effective gas permeability at final water saturation versus K_{inf}. Also for K_{ro} and K_{rw} versus saturation for all lithofacies.
4- Because capillary pressure data depend on interfacial tension between the fluid phases present, data obtained in the laboratory under conditions different from those in the reservoir must be adjusted for interfacial tension.
5- The water saturation at the outlet face of the individual core plugs is smaller than the average water saturation in the sample. This was not the case for Plug 80S (S_{ofave} = 0.4872 frac PV and S_{ofFace}=0.2588 frac PV). We do not have an explanation for this behavior.
6- The heterogeneities' existence affects the steady state Pc versus saturation curves. That is the major reason to upscale flow behavior from the core to the field scale to design oil recovery manners. So, particular concern must be considered not to disregard these heterogeneities; else the field simulation outcomes to be based on the kind, consistency, and distribution of heterogeneities may be evaluated improperly. The tests, e.g. CT scanning rocks or other radioactivity and resistivity logging tools such as gamma-ray logging, are required to estimate the kinds and how heterogeneity is distributed in the formation to demonstrate saturation distribution in and at the end of the fluid flow period.
7- The rock type does not seem to influence the flow relationships other than its wetting preference. However, according to the surface minerals, most of the time carbonate rocks are oil wet while sandstones are usually water wet. In addition, carbonates usually have vugs and when large vugs exist in the reservoir, the core sample used in the experiment might not be representative of the reservoir. When laboratory data of carbonates is being used to predict three-phase flow, a greater uncertainty has been noticed. Attention must be paid to the assumptions of the model to select the appropriate one for carbonates and sandstones.

Acknowledgments

This study was established under supervision of Amirkabir University of Technology/ Petroleum Engineering Department and University of Baghdad/ Petroleum Engineering Department as a part of Ph.D. dissertation on Mishrif Formation in West Qurna oilfield, Southern Iraq. The authors would like to thank Basrah Oil Company (BOC) and all Engineers and Geologists in Iraqi Ministry of Oil and Ministry of Higher Education and Scientific Research.

Nomenclature

BV	Bulk volume
℃	Degrees Celsius
CT	Computerized tomography
℉	Degrees Fahrenheit
Frac.	Fraction
g/cc	Grams per cubic centimeter
JBN	Johnson, Bossler, Naumann method for unsteady-state relative permeability data
k	Absolute Permeability *(dimensionless)*
k_g	Gas Permeability (*md)*
k_{ge}	Gas Effective Permeability (*md)*
K_{inf}	Klinkenberg-corrected permeability (*md)*
k_o	Oil permeability (*md)*
k_{oe}	Oil effective permeability (*md)*
k_{rb}	Brine relative permeability *(dimensionless)*
k_{rg}	Gas relative permeability *(dimensionless)*
k_{ro}	Oil relative permeability *(dimensionless)*
k_{rw}	Water relative permeability *(dimensionless)*
Pc	Capillary Pressure *(psi)*
ppm	Parts per million
psi	Pounds per square inch
m	Porosity Exponent *(dimensionless)*
md or mD	mille-Darcy
n	Saturation Exponent *(dimensionless)*
NCS	Net confining stress *(psi)*
n_i	Corey exponent for the displacing phase i *(dimensionless)*
n_{ij}	Corey exponent for phase i being displaced by phase j *(dimensionless)*
rc	Effective radius of the porous media *(inch)*
Ro	Core sample resistivity *(ohm-m)*
Rw	Formation brine resistivity *(ohm-m)*
S_g	Gas saturation *(Frac.)*
S_{gr}	Residual gas saturation *(Frac.)*
S_o	Oil saturation *(Frac.)*
S_{oi}	Initial oil saturation *(Frac.)*
S_{on}	Normalized oil saturation *(Frac.)*
S_{or}	Remaining (or residual) oil saturation *(Frac.)*
S_{org}	Residual oil saturation to gas drive at

	Pc,go = +∞ *(Frac.)*
S_{orw}	Residual oil saturation to water drive at Pc,wo = -∞ *(Frac.)*
SS	Steady-state method for conducting relative permeability tests *(dimensionless)*
Sw	Water saturation *(Frac.)*
S_{wi}	Initial water saturation *(Frac.)*
S_{wf}	Final water saturation *(Frac.)*
S_{wir}	Irreducible water saturation at Pc, WO = +∞ *(Frac.)*
S_{wr}	Normalized water saturation *(Frac.)*
Sx	Non-wetting saturation *(Frac.)*
TDS	Total dissolved solids
USS	Unsteady-state method for conducting relative permeability tests *(dimensionless)*
θ	Contact angle *(degree)*
ρ_g	Grain density *(gm/cc)*
σ	Interfacial Tension *(lb/in)*
φ	Porosity *(Frac.)*

References

[1] Hutchinson, C. A., C. F. Dodge, and T. L. Polasek. "Identification, classification and prediction of reservoir nonuniformities affecting production operations." *Journal of Petroleum Technology* 13.03, 1961, pp 223-230. https://doi.org/10.2118/1576-G-PA.

[2] Zeito, George A. "Interbedding of shale breaks and reservoir heterogeneities." *Journal of Petroleum Technology* 17.10, 1965, pp 1223-1228. https://doi.org/10.2118/1128-PA.

[3] Dodge, Charles F., Dennis P. Holler, and Robert L. Meyer. "Reservoir heterogeneities of some Cretaceous sandstones." *AAPG Bulletin* 55.10, 1971, pp 1814-1828. https://doi.org/10.1306/819A3DAA-16C5-11D7-8645000102C1865D.

[4] McClure, James E., et al. "The LBPM software package for simulating multiphase flow on digital images of porous rocks." *Computational Geosciences* 25.3, 2021, pp 871-895. https://doi.org/10.1007/s10596-020-10028-9.

[5] Al-Sudani, Jalal Abdulwahid, Rwaida Kaiser, and Salam J. Al-Rubeai. "Estimation liquid permeability using air permeability laboratory data." *Iraqi Journal of Chemical and Petroleum Engineering* 15.1, 2014, pp 43-50.

[6] Semnani, Ali Khosravani, Hamidreza Shahverdi, and Ali Reza Khaz'ali. "Averaging the experimental capillary pressure curves for scaling up to the reservoir condition in the imbibition process." *Journal of Petroleum Science and Engineering* 184, 2020: 106539. https://doi.org/10.1016/j.petrol.2019.106539.

[7] Hosseinzadeh, Sirous, Ali Kadkhodaie, and Saeed Yarmohammadi. "NMR derived capillary pressure and relative permeability curves as an aid in rock typing of carbonate reservoirs." *Journal of Petroleum Science and Engineering* 184, 2020: 106593. https://doi.org/10.1016/j.petrol.2019.106593.

[8] Hu, Xuetao, and Su Huang. "Physical properties of reservoir rocks." *Physics of petroleum reservoirs*. Springer, Berlin, Heidelberg, 2017, pp 7-164. https://doi.org/10.1007/978-3-662-53284-3_2.

[9] Liu, Siyan, et al. "Application of neural networks in multiphase flow through porous media: Predicting capillary pressure and relative permeability curves." *Journal of Petroleum Science and Engineering* 180, 2019, pp 445-455. https://doi.org/10.1016/j.petrol.2019.05.041.

[10] R. F. John "Principles of applied reservoir simulation". Elsevier, 1-12, 2001. https://doi.org/10.1016/B978-075067933-6/50003-9.

[11] Bear, Jacob. *Modeling phenomena of flow and transport in porous media*. Vol. 1. Cham: Springer International Publishing, 2018. https://doi.org/10.1007/978-3-319-72826-1.

[12] Pini, Ronny, and Sally M. Benson. "Simultaneous determination of capillary pressure and relative permeability curves from core-flooding experiments with various fluid pairs." *Water Resources Research* 49.6, 2013, pp 3516-3530. https://doi.org/10.1002/wrcr.20274.

[13] Moura, M., et al. "Impact of sample geometry on the measurement of pressure-saturation curves: Experiments and simulations." *Water Resources Research* 51.11, 2015, pp 8900-8926. https://doi.org/10.1002/2015WR017196.

[14] Amyx, James, Dantel Bass, and Robert L. Whiting. *Petroleum reservoir engineering physical properties*. 1960.

[15] Li, Yong, et al. "A fast method of waterflooding performance forecast for large-scale thick carbonate reservoirs." *Journal of Petroleum Science and Engineering* 192, 2020: 107227. https://doi.org/10.1016/j.petrol.2020.107227.

[16] Muntadher, AL-Nafie. "Estimation of reservoir properties based on core plugs, lithofacies, and well logs for Nahr Umr Formation in Noor oilfield, southern Iraq." *Iraqi Journal of Science* (2022). https://doi.org/10.24996/ijs.2022.63.5.22.

[17] Schäfer, Gerhard, et al. "On the prediction of three-phase relative permeabilities using two-phase constitutive relationships." *Advances in Water Resources* 145, 2020: 103731. https://doi.org/10.1016/j.advwatres.2020.103731.

[18] Foroudi, Sina, Alireza Gharavi, and Mobeen Fatemi. "Assessment of two-phase relative permeability hysteresis models for oil/water, gas/water and gas/oil systems in mixed-wet porous media." *Fuel* 309, 2022: 122150. https://doi.org/10.1016/j.fuel.2021.122150.

[19] Blunt, Martin J. "Flow in porous media—pore-network models and multiphase flow." *Current opinion in colloid & interface science* 6.3 (2001): 197-207. https://doi.org/10.1016/S1359-0294(01)00084-X.

[20] Leverett, Ml C. "Flow of oil-water mixtures through unconsolidated sands." *Transactions of the AIME* 132.01, 1939, pp 149-171. https://doi.org/10.2118/939149-G.

[21] Hassler, G. L., and E. Brunner. "Measurement of capillary pressures in small core samples." *Transactions of the AIME* 160.01, 1945, pp 114-123. https://doi.org/10.2118/945114-G.

[22] Borazjani, S., et al. "Determining water-oil relative permeability and capillary pressure from steady-state coreflood tests." *Journal of Petroleum Science and Engineering* 205, 2021: 108810. https://doi.org/10.1016/j.petrol.2021.108810.

[23] Abeysinghe, Kumuduni Prasangika, Ingebret Fjelde, and Arild Lohne. "Dependency of remaining oil saturation on wettability and capillary number." *SPE* Saudi Arabia Section Technical Symposium and Exhibition. OnePetro, 2012. https://doi.org/10.2118/160883-MS.

[24] Hirasaki, G. J., J. A. Rohan, and J. W. Dudley. "Interpretation of oil-water relative permeabilities from centrifuge experiments." *SPE* Advanced Technology Series 3.01, 1995, pp 66-75. https://doi.org/10.2118/24879-PA.

[25] Ren, Jie, Yuan Wang, and Di Feng. "Competitive Effects of Permeability and Gravity on the Drying-Out Process during CO2 Geological Sequestration in Saline Aquifers." *Lithosphere* 2021.Special 4, 2022: 3198305. https://doi.org/10.2113/2022/3198305.

[26] Baker, L. E. "Three-phase relative permeability correlations." *SPE* Enhanced Oil Recovery Symposium. OnePetro, 1988. https://doi.org/10.2118/17369-MS.

[27] Bear, Jacob, and Carol Braester. "On the flow of two immscible fluids in fractured porous media." *Developments in Soil Science*. Vol. 2. Elsevier, 1972, pp 177-202. https://doi.org/10.1016/S0166-2481(08)70538-5.

[28] Zhai, Zhiwei, et al. "Experimental studies on influence of temperature on relative permeability curves in sandstone reservoirs." *Energy Exploration & Exploitation* 40.1, 2022, pp 206-223. https://doi.org/10.1177%2F01445987211040876.

[29] Finlayson, L., et al. "Applications of New Wireline Technology in a Mature Middle-East Oil Field." First EAGE Workshop on Iraq-Hydrocarbon Exploration and Field Development. *European Association of Geoscientists & Engineers*, 2012. https://doi.org/10.3997/2214-4609.20143568.

[30] Mahdi, Thamer A., et al. "Sedimentological characterization of the mid-Cretaceous Mishrif reservoir in southern Mesopotamian Basin, Iraq." *GeoArabia* 18.1, 2013, pp 139-174. https://doi.org/10.2113/geoarabia1801139.

[31] Al-Dujaili A.N., Shabani M., and AL-Jawad M.S. "Identification of the best correlations of permeability anisotropy for Mishrif reservoir in West Qurna/1 Oil Field, Southern Iraq", *Egyptian Journal of Petroleum*, 2021a, pp 27-33. https://doi.org/10.1016/j.ejpe.2021.06.001.

[32] Aqrawi, A. A. M., et al. "Characterization of the Mid-Cretaceous Mishrif reservoir of the southern Mesopotamian Basin, Iraq". *American Association of Petroleum Geologists Conference and Exhibition*. Seven, 2010.

[33] Thamer A. Mahdi, Adnan A.M. Aqrawi, Andrew D. Horbury, Govand H. Sherwani "Sedimentological characterization of the mid-Cretaceous Mishrif reservoir in southern Mesopotamian Basin, Iraq". GeoArabia. 18 (1), 2013, pp 139–174. https://doi.org/10.2113/geoarabia1801139.

[34] Al-Dujaili, A.N., Shabani, M. & AL-Jawad, M. S. "Characterization of flow units, rock and pore types for Mishrif Reservoir in West Qurna oilfield, Southern Iraq by using lithofacies data". *J Petrol Explor Prod Technol*, 2021, pp 4005–4018. https://doi.org/10.1007/s13202-021-01298-9.

تأثير عدم التجانس على الضغط الشعري ومنحنيات النفاذية النسبية في المكامن الكربونية. دراسة حالة لتكوين مشرف في حقل غرب القرنة / ١ ، العراق

أحمد نوري الدجيلي [١]، مهدي شعباني [١،*]، ومحمد صالح الجواد [٢]

١ جامعة أمير كبير التكنولوجية، قسم هندسة النفط، ايران
٢ قسم هندسة النفط، كلية الهندسة، جامعة بغداد، العراق

الخلاصة

تم إجراء اختبارات التحليل الأساسية الخاصة (SCAL) على مجموعة من النماذج الصخرية لتكوين مشرف (وحدات mA و mB1 و mC / mB2cde) في حقل غرب القرنة / ١، جنوب العراق. تم استخدام بيانات النفاذية النسبية للزيت (Kro) ومعادلات كوري كوظائف لتشبع المحلول الملحي في مقدمة المخرج الأساسي للعينات الفردية عند عملية تشرب الماء والزيت لحساب النفاذية النسبية بواسطة طريقة الطرد المركزي. تم استخلاص الارتباطات المتطابقة للنفاذية النسبية للزيت والماء بواسطة طريقتي الحالة المستقرة والحالة غير المستقرة. بالنسبة لعينات وحدة (mA) ، وقعت منحنيات الضغط الشعري للغاز والماء ضمن نطاق ضيق (متطابق تقريبًا) مما يشير إلى أن هذه الوحدة هي وحدة متجانسة. كانت منحنيات Kro لثلاثة عينات صخرية لوحدة mB2ab متطابقة عمليًا، وهذا يشير إلى التجانس في الجزء العلوي من الوحدة.

تحتوي وحدة mB2 على تركيز طور أكثر صلابة من الوحدات الأخرى. بالإضافة إلى ذلك ، يرتبط الاتجاه العام لانخفاض التشبع للزيت المتبقي بزيادة المسامية ولكن لا توجد علاقة موثوقة بين تشبع الزيت المتبقي بتشبع (Sorw) ونفاذية Klinkenberg المصححة (Kinf). استنادًا إلى العلاقة بين نفاذية الزيت الفعالة عند تشبع الماء الأولي [ko (Swi)] و $(Kinf/f)^{1/2}$)، للنماذج الصخرية لوحدة mB1 ذات النفاذية العالية، فإن ko (Swi) يساوي تقريبًا Kinf أو يتجاوزه، بينما كان أقل من Kinf للعينات الأخرى. تم الحصول على معادلات تجريبية جديدة جيدة لنفاذية الغاز الفعالة عند تشبع الماء النهائي مقابل Kinf ومعادلات تربط بين Kro و Krw مقابل التشبع لجميع النماذج الصخرية

الكلمات الدالة: عدم التجانس، النفاذية النسبية، الضغط الشعري، مشرف، غرب القرنة، الاستخلاص الثانوي، قابلية التبلل.